Thermodynamic and dynamic responses of the hydrological cycle to solar dimming

Jane E. Smyth[1], Rick D. Russotto[2], and Trude Storelvmo[1]

[1]Department of Geology & Geophysics, Yale University, New Haven, Connecticut, USA
[2]Department of Atmospheric Sciences, University of Washington, Seattle, Washington, USA

Correspondence to: Jane E. Smyth (jsmyth@princeton.edu)

Abstract. The fundamental role of the hydrological cycle in the global climate system motivates thorough evaluation of its responses to climate change and mitigation. The Geoengineering Model Intercomparison Project (GeoMIP) is a global collaboration that aims to assess the climate impacts of solar geoengineering, a proposal to counteract global warming with a reduction of incoming solar radiation. We assess the mechanisms underlying the rainfall response to a simplified simulation of solar dimming (G1) in the suite of GeoMIP models and identify robust features. While solar geoengineering nearly restores preindustrial temperatures, the global hydrology is altered. Tropical precipitation changes dominate the response across the model suite, and these are driven primarily by shifts of the Hadley circulation cells. We report a damping of the seasonal migration of the intertropical convergence zone (ITCZ) in G1, associated with preferential cooling of the summer hemisphere, and annual mean ITCZ shifts in some models that are correlated with warming of one hemisphere relative to the other. These dynamical changes cause greater rainfall anomalies than local changes in relative humidity or the Clausius-Clapeyron scaling of precipitation minus evaporation. The role of relative humidity, though small in the zonal mean, could be locally important over land, and is likely related to the CO_2 physiological response in plants. The variations among models in the movement of the intertropical convergence zone highlights the need for cautious consideration and continued study before any implementation of solar geoengineering.

1 Introduction

Solar geoengineering has been suggested as a way to counter the effects of global warming induced by anthropogenic greenhouse gas emissions (e.g., Crutzen, 2006; Robock et al., 2009). By reducing incoming solar radiation, solar geoengineering would bring the climate with elevated concentrations of CO_2 into radiative balance. It compensates for a change in surface temperature from increased CO_2 trapping of outgoing longwave radiation with a reduction of incoming shortwave radiation. Solar geoengineering is a controversial proposal, but should it come into favor due to continued greenhouse gas emissions, it is critical that the climate effects be understood before deployment (NRC, 2015).

The Geoengineering Model Intercomparison Project (GeoMIP) is intended to determine robust responses of the climate to various simulations of solar geoengineering, in experiments that range from simple representations of the solar dimming, to realistic representations of stratospheric aerosol emissions or marine cloud brightening (Kravitz et al., 2010). The GeoMIP

experiments are based on the Coupled Model Intercomparison Project Phase Five (CMIP5), which is a protocol for experiments using coupled atmosphere-ocean climate models (Table 1). The GeoMIP G1 experiment counteracts the forcing from quadrupled atmospheric CO_2 levels with a simple reduction of the solar constant across all wavelengths. The G1 experiment was run from the steady state preindustrial control (piControl) run, followed by an abrupt quadrupling of CO_2, and a simultaneous solar constant reduction for 50 years. The idealized nature of this simulation is conducive to multimodel comparison. It superimposes two large and opposite climate forcings, which offset one another nearly completely in terms of global mean net radiation balance at the top of the atmosphere and near-surface atmospheric temperature, but do not cancel in their hydrological effects, especially on local scales (Kravitz et al., 2013c).

Thirteen fully coupled models participated in the G1 experiment, though we did not have access to the data from the CSIRO model and it is not included in the present study. There are serious errors in the precipitation output files from the EC-EARTH model and it is thus excluded from any analysis involving the precipitation field. The models differ in their ocean, ice sheet, land surface and atmospheric components. The latter two components are particularly relevant for this study. Some, but not all models, feature dynamic vegetation distributions. The 11 models include a wide range of parametrizations and configurations, allowing for strong conclusions about robust climate responses that appear across models (Kravitz et al., 2013a).

The water cycle impacts agriculture, economies, as well as the welfare of ecosystems and human civilizations (IPCC, 2014). It is imperative to understand the effects of solar geoengineering on global hydrology, to evaluate whether the risks or unintended consequences of such an approach to climate change mitigation are likely to outweigh the benefits. To help improve our understanding of this issue, we analyze the contributions of several different effects to changes in precipitation minus evaporation ($P - E$) in the GeoMIP G1 experiment, as follows.

1. In Section 2.1, we analyze the thermodynamic response of $P - E$ to geoengineering.
2. In Section 2.2, we assess the role of changes in relative humidity on $P - E$.
3. In Section 2.3, we investigate the extent to which atmospheric circulation patterns, namely changes in the Hadley cell strength and position, drive $P - E$ changes in the models on both annual and seasonal timescales.

2 Analysis & Results

2.1 Thermodynamic Scaling of $P - E$

Precipitation minus evaporation determines the amount of subsurface and surface runoff on land, and is crucial in setting the salinity of the mixed layer over ocean (Byrne and O'Gorman 2015). We here discuss the component of $P - E$ changes driven by residual surface temperature changes (G1- piControl). Surface heating increases the temperature and the evaporation rate, which increases the atmospheric moisture content, or specific humidity q (Trenberth, 1999). We have confidence about certain aspects of the hydrological cycle's response to greenhouse gas warming, particularly those tightly coupled to the increase in saturation vapor pressure with warming (Held and Soden, 2006). The Clausius-Clapeyron expression (Eq. (1)), where R is

the gas constant, L the latent heat of vaporization, and α is the Clausius-Clapeyron scaling factor, relates the derivative of the natural log of saturation vapor pressure e_s with respect to temperature (T) to temperature itself.

$$\frac{d\ln e_s}{dT} = \frac{L}{RT^2} \equiv \alpha(T) \tag{1}$$

At typical near-surface temperatures, saturation vapor pressure increases at 7 $\%\mathrm{K}^{-1}$.

Precipitation minus evaporation follows Clausius-Clapeyron scaling, as in Eq. (2), given three important assumptions (Held and Soden, 2006).

$$\delta(P-E) = \alpha\,\delta T\,(P-E) \tag{2}$$

First, it assumes small meridional gradients of temperature relative to $P-E$. Second, the relationship assumes no change in near-surface relative humidity between climate states. Third, it assumes that there is no change in the atmospheric flow. Though it is known that relative humidity and atmospheric circulation are not constant in a changing climate, the thermodynamic scaling is a useful way to represent the role of a simple physical mechanism (i.e. the Clausius-Clapeyron scaling of saturation vapor pressure with temperature) on global $P-E$ anomalies (Byrne and O'Gorman, 2015). This thermodynamic scaling equation represents the component of $P-E$ change driven directly by surface temperature perturbations. $P-E$ changes not captured by this scaling are driven by non-thermodynamic mechanisms, including changes in relative humidity or atmospheric dynamics.

This study evaluates the extent to which the basic physical relation between saturation vapor pressure and temperature accounts for the hydrological response to a combination of large-magnitude forcings: greenhouse gas warming and solar dimming.

We investigate how well thermodynamic scaling predicts hydrologic changes in a geoengineered climate for each model by comparing the prediction using Eq. (2) to the annual and zonal mean $P-E$ anomaly between G1 (years 11-50) and piControl (all years) in the model simulations. We also consider the annual-mean global distribution of precipitation minus evaporation anomalies. To better understand the contribution of relative humidity changes to the $P-E$ response, we also calculated an "extended scaling" adapted from Byrne and O'Gorman (2015). Our extended scaling includes the first two terms from Byrne and O'Gorman's equation,

$$\delta(P-E) = \alpha\,\delta T\,(P-E) + \frac{\delta H_s}{H_s}\,(P-E) \tag{3}$$

where H_s is the relative humidity at the surface. The calculation takes local changes in H_s into account, but for the sake of simplicity it excludes changes in the horizontal gradients of H_s. We calculated the difference between the zonal mean $P-E$ anomalies in the extended and simple scalings to quantify the influence of changes in H_s. We also calculated the difference between simulated $P-E$ anomalies and the extended thermodynamic scaling, to isolate the role of dynamics in the simulated hydrological response. Data for this analysis and the relative humidity analysis in Section 2.2 were unavailable for CESM, HadC, and MPI due to limited functionality of the central GeoMIP model data server, the Earth System Grid Federation (ESGF).

To provide reference points for our analysis, we have re-plotted some thermodynamic variables in Figures 1-3 that originally appeared in the G1 overview paper by Kravitz et al. (2013a). The experimental design results in minimal temperature anomalies between G1 (years 11-50) and piControl(all years) (Fig. 1), but does not eliminate hydrological effects (Fig. 2). The ensemble mean change in $P-E$ shows greater hydrological changes (up to 1 mm/day) in the tropics than at higher latitudes (Fig. 2). Figure 3, which separates the precipitation and evaporation changes from solar dimming, reveals that most of the spatial structure in the $P-E$ anomaly comes from the precipitation change.

The thermodynamic scaling captures virtually no change in global $P-E$ patterns, since by experimental design the temperature anomaly is minimal between the G1 and piControl scenarios (Fig. 4B). Temperature anomalies between G1 and the piControl show variations within 1 K, with some residual warming at high latitudes and cooling at low latitudes as a robust feature across the suite (Fig. 1) (Kravitz et al. 2013a). Such temperature anomalies are generally not sufficient to generate appreciable thermodynamic changes in P-E. The ensemble mean simulated precipitation minus evaporation anomaly deviates from the thermodynamic scaling by up to 1.0 $\mathrm{mm/day}$ and is highest in the tropics (Fig. 2). In the tropics,temperature anomalies are minimal compared to those at high northern latitudes and thus thermodynamic scaling does not account for the hydrological change. In BNU-ESM, thermodynamic scaling predicts a $P-E$ enhancement over the anomalously warm high latitudes, where the temperature response to quadrupled CO_2 levels is poorly compensated by solar dimming (annual mean G1-piControl anomalies >2K at polar latitudes, results not shown here).

The ensemble mean reflects strong reductions in precipitation in the subtropics (Fig. 3). Previous research has suggested that this is a result of the nature of the G1 experiment forcing. Solar geoengineering might suppress tropical precipitation since the reduction in shortwave radiation cools the surface more than the mid-troposphere, increasing atmospheric stability and reducing convection (Bala et al., 2008). However, looking at the zonal patterns for individual models, there are stronger hydrological effects that cancel out in the ensemble mean (Fig. 4A). The HadCM3, HadGEM2-ES, and CESM-Cam5.1-FV models show P-E anomalies indicating a northward shift in the Intertropical Convergence Zone (ITCZ), while those of GISS-E2-R, Can-ESM2, and MIROC-ESM demonstrate a southward shift. Annual mean anomalies in the zonal mean $P-E$ exceed 0.6 $\mathrm{mm/day}$ in the GISS-E2-R and HadGEM2-ES simulations. In CCSM4, IPSL-CM5A-LR, and NorESM1-M models, the ITCZ appears to narrow, with precipitation increasing at the equator and decreasing within 10°N and 10°S.

The deviations of the extended scaling from the simple scaling are less than 0.1 $\mathrm{mm/day}$ in all models (Fig. 4C). This demonstrates that local changes in relative humidity under solar dimming play a modest role in the zonal mean $P-E$ response. Figure 4D indicates that most of the zonal mean $P-E$ anomalies are not captured by the Clausius-Clapeyron scaling or by local relative humidity changes. We interpret this component of the hydrological response to be driven by atmospheric circulation changes. To better understand the influence of relative humidity changes on smaller spatial scales, we investigate the global distribution of H_s changes in the following section. We will then investigate the dynamical changes in the tropics in Section 2.3.

2.2 Relative Humidity

The thermodynamic scaling described above assumes no changes in relative humidity between climate states. In this section, we assess the role that relative humidity changes play in the $P-E$ response to uniform solar dimming. Relative humidity is the ratio of actual vapor pressure to saturation vapor pressure ($\frac{e}{e_s}$), or almost equivalently, specific humidity to saturation specific humidity ($\frac{q}{q_s}$). It can change with the water availability or temperature, with the latter affecting the saturation vapor pressure as in Eq. (1). The near-surface atmosphere provides moisture to the free troposphere, where water vapor plays an important role in radiative transfer, the hydrological cycle, and climate sensitivity (Willett et al., 2010). The near-surface relative humidity parameter is also of interest in climate change studies for evaluating the risk of human heat stress, under both high and low H_s extremes (Sherwood et al., 2010; Souch and Grimmond, 2004).

The assumption of constant relative humidity in the simple thermodynamic scaling of $P-E$ (Eq. (2)) relies on the availability of moisture. In a moisture-limited regime (i.e., over land) q may not increase proportionally with temperature, breaking the assumption of constant relative humidity. Under this circumstance, relative humidity adjustments would contribute to non-thermodynamic changes in the $P-E$ between climate states. An observational study found decreasing surface relative humidity from 1998-2008 over low and midlatitude land areas due to inhomogeneities in surface heating and moisture availability (Simmons et al., 2010). While relative humidity has been found to be nearly constant in global warming simulations with high vertical resolution (Allen and Ingram, 2002), the assumption of constant H_s may not be sound when insolation rather than temperature is perturbed, as in the G1 experiment.

We consider the absolute changes in the relative humidity distribution to explain precipitation anomalies between G1 (years 11-50) and piControl (all years) simulations unaccounted for by thermodynamic or dynamic mechanisms. As noted in Section 2.1, the relative humidity data were unavailable for the CESM, HadC, and MPI models due to limited functionality of the ESGF data server. In six of the eight models presented here, relative humidity is reduced over land and conserved over ocean (Fig. 5). The relative humidity reductions are largest over tropical South America and sub-Saharan Africa. The reductions are up to 15% (0.15) in GISS-E2-R and HadGEM2-ES (calculated as the G1 relative humidity (%) minus the piControl relative humidity (%)). The CO_2 physiological effect is included in the land models of 11 GeoMIP simulations, all but EC-Earth (Table 1). In response to elevated ambient CO_2 concentrations, plants constrict their stomata, which reduces evapotranspiration in the high CO_2 simulations, including the G1 simulations (Kravitz et al., 2013c; Cao et al., 2010). In the global warming (abrupt4xCO2) GeoMIP simulations, this effect is partially offset by the increased net primary productivity in a warmer world. However, in G1, this net primary productivity effect is muted by the reduction in insolation. Tilmes et al. (2013) found that the physiological response to G1 is qualitatively the same as for abrupt4xCO2. Biogeochemical cycling has been found to influence global precipitation as much as the radiative reduction itself (Fyfe et al., 2013).

Bala et al. (2008) investigated changes in global mean precipitation in a single climate model. They noted a greater hydrological sensitivity to solar versus greenhouse forcing and attributed it to global energy budget constraints. Solar forcing heats the surface directly, while greenhouse forcing heats the troposphere. Changes in the insolation therefore have a greater effect on surface net radiation fluxes (i.e., latent and sensible heat fluxes change more than in the CO_2 case). When the downward

shortwave flux decreases, the surface fluxes must respond, and in this case the latent heat flux dominates the response. Evaporation decreases, and precipitation follows. Bala et al. do not address how this global mean equilibrium constraint will manifest regionally, but our analysis (e.g. Fig 3) is consistent with this reasoning.

In the National Center for Atmospheric Research (NCAR) Community Land and Community Atmosphere Model, Cao et al. (2010) isolated the CO_2 physiological effect from a doubling of atmospheric CO_2. They reported patterns of reduced latent heat flux and relative humidity from this vegetative forcing that closely resemble those we observe in the GeoMIP suite, in Fig. 3 and Fig. 5. In the present study, since strong and significant reductions in relative humidity over land are largely constrained to regions with extensive vegetation in the form of boreal, temperate or tropical forests, we consider the biogeochemical effect of CO_2 to be the dominant cause of the relative humidity change. The role of these biogeochemical H_s changes is minimal in zonal mean climate (Fig. 4C) but could have significant influence at smaller spatial and temporal scales.

2.3 Dynamically Driven Precipitation

The third factor we consider in decomposing the $P-E$ response to geoengineering is the atmospheric circulation. Large-scale meridional circulations are driven by energy gradients imposed by the uneven distribution of sunlight on Earth. The Hadley circulation cells are responsible for most of the poleward heat transport in the tropics, where the annual solar input is highest (Hill et al., 2015). The net energy flux of the Hadley circulation is in the flow direction of its upper branch (Held, 2001). The ascending motion of the Hadley cell drives the seasonally-migrating tropical rainfall known as the ITCZ, and there is evidence that its position is determined by meridional gradients in the vertically-integrated atmospheric energy budget (Shekar and Boos, 2016). The Hadley circulation is crucial for balancing global energy, so high-latitude temperature anomalies can drive shifts of the ITCZ (Yoshimori and Broccoli, 2008). The ITCZ is sensitive to interhemispheric energy contrasts set up by aerosols, clouds, or antisymmetric heating (Seo et al., 2014). A thorough analysis of Hadley circulation changes is a crucial outstanding task for understanding the hydrological response to solar geoengineering (Kravitz et al., 2013c). We will quantify changes to the Hadley circulation with the meridional streamfunction. The meridional streamfunction is derived from the continuity equation, and either $\bar{v}$, the meridional wind vector, or $\bar{w}$, the vertical wind vector, can be used to fully define the two-dimensional, overturning flow (Eq. (4)):

$$\Psi(\phi,p) = 2\pi a \cos\phi \int_0^p \bar{v}\,\mathrm{d}p/g. \tag{4}$$

where ϕ is the latitude, p is pressure, a is the Earth's radius, $\bar{v}$ is the meridional velocity, and g is gravity.

Changes in TOA energy fluxes influence the direction and strength of ITCZ shifts (Kang et al., 2008). Numerous studies have noted the strong relationship between ITCZ position and the hemispheric temperature contrast as well. The correlation between interhemispheric temperature contrasts and annual mean ITCZ position is a robust result and is related to extratropical energy transport (e.g., Broccoli et al., 2006; Toggweiler and Lea, 2010). Schneider et al. (2014) explain how this is consistent with an energetic framework: the hemisphere with the higher average temperature typically has a smaller meridional temper-

ature gradient due to the near symmetry of tropical temperatures about the equator. This corresponds to reduced poleward extratropical eddy transport in that hemisphere, and increased energy flux by the atmosphere across the equator and out of the hemisphere by the upper branch of the Hadley cell. The ITCZ is drawn towards the warmed hemisphere because moisture is transported in the opposite direction as energy by the Hadley cell. Therefore, we investigate the possibility that differing dynamical responses to solar dimming among the models are due to differences in the temperature restoration of the Northern and Southern Hemispheres.

To discern the component of the precipitation change caused by changes in large scale atmospheric dynamics, we calculated the change in the Hadley circulation between the G1 (years 11-50) and piControl (final 40 years) simulations. For each model, we computed the meridional streamfunction over this 40 year averaging period based on the modeled meridional wind vector, as in Eq. (4). Data were unavailable for the CESM and HadC models. We examined annual and seasonal mean dynamical changes to analyze the changes in the zonal mean hydrological cycle, including the periods July-August-September (JAS) and January-February-March (JFM). To better interpret the dynamical changes, we assessed the annual mean and seasonal changes in the interhemispheric temperature contrast between G1 and piControl for each model by calculating area-weighted hemispheric averages of the surface temperature, averaged over a 40 year period (years 11-50 of G1 and 1-40 of piControl). The ITCZ shift between G1 and piControl is defined as the shift of the precipitation centroid. This is the latitude between 15°N and 15°S at which half the precipitation is to the north and half is to the south.

The annual mean Hadley circulation changes vary in magnitude and direction amongst the GeoMIP ensemble members and contribute to dynamic moistening and drying. The meridional streamfunction plots suggest that the northward (HadGEM2-ES) and southward (GISS-E2-R, MIROC-ESM) ITCZ shifts, characterized by counterclockwise or clockwise tropical anomalies respectively, are dynamically driven (Fig. 6). The anomalous ascent at the equator in CCSM4 and NorESM1-M accounts for the narrowing of the ITCZ noted in the zonal mean $P-E$ figure. The mean circulation does not seem to provide a dynamical basis for the annual mean constriction of the ITCZ in the MPI-ESM-LR and IPSL-CM5A-LR models, in which anomalies are less than 10^{10} kg s^{-1}. Small changes in the latitudinal range and strength of the Hadley circulation and associated precipitation have large local implications, especially on subannual scales (Kang et al., 2009). We find that summer (July-August-September, or JAS) and winter (January-February-March, or JFM) meridional streamfunction anomalies are in every model stronger than the annual mean (Figs. 7, 8). In HadGEM2-ES, for example, the JAS meridional mass flux anomaly exceeds 4×10^{10} kg s^{-1}. On the opposite extreme, the IPSL-CM5A-LR model JAS and JFM mass flux anomalies are below 1.5×10^{10} kg s^{-1}. In general, the JAS streamfunction changes rather than the JFM anomalies set the pattern for the annual mean circulation change (Figs. 6-8). In the JAS average, there is anomalous energy transport toward the summer hemisphere (NH) in eight of nine models (all but HadGEM) (Fig. 7). In the JFM average, there is again anomalous energy transport toward the summer hemisphere (SH), though the result is less consistent across the suite (seven of nine models) (Fig. 8). These changes in the Hadley cell mass flux are consistent with the relative cooling of the summer hemisphere throughout the year (Fig. 9b,c).

We find that the shifts of annual mean tropical rainfall in the models are correlated with the interhemispheric surface temperature contrasts (Correlation coefficient $(r) = 0.64$, Fig. 9a). Models with higher annual mean surface temperatures in the Northern Hemisphere under geoengineering tend to display northward shifts of the ITCZ. This is consistent with previous

research that shows a strong relationship between the ITCZ position and the hemispheric temperature contrast (e.g., Kang et al., 2008; Frierson and Hwang, 2012). Modeling studies by Haywood et al. (2013, 2016) have shown that increasing the albedo by injecting stratospheric aerosols into only one hemisphere could cause substantial shifts in the ITCZ toward the other hemisphere. Our analysis of the G1 experiment suggests that similar effects could occur, albeit on a smaller scale, even with a hemispherically symmetric injection strategy, which is approximated by reducing the solar constant. Despite the hemispherically symmetric forcing induced by solar dimming, the ensemble mean residual high-latitude warming is larger in the Arctic than in the Antarctic (Fig. 1), and in 9 out of 11 models the Northern Hemisphere is warmed relative to the Southern Hemisphere after geoengineering (Fig. 7a). This suggests that there could be an intriguingly close relationship between the degree of Arctic warming amplification and the tropical hydrological response to geoengineering in models. The relationship between ITCZ shifts and energy transport in G1 will be further explored in a future study.

One response of the ITCZ to the G1 experiment that is consistent across all 11 models is that the seasonal migration of the ITCZ is dampened. Figure 10 shows the annual, boreal winter (JFM), and boreal summer (JAS) mean position of the ITCZ in each model in piControl (years 1-40) and G1 (years 11-50). In each model, the distance between the seasonal mean positions of the ITCZ is reduced. In some models there is a poleward shift in the ITCZ in one of the seasons, but in each of these cases there is a greater equatorward shift in the opposite season, with an annual mean ITCZ shift and a reduction in the seasonal migration occurring simultaneously.

The reduction in the seasonal ITCZ migration is consistent with the physical mechanism relating sulfate aerosols and ITCZ shifts during 1971-1990 described by Hwang et al. (2013; see their Figure 4). There is more available sunlight in the summer hemisphere, which results in a greater cooling there when the solar constant is reduced. To compensate for the loss of energy in the summer hemisphere, the climatological energy flux out of the summer hemisphere and towards the winter hemisphere is reduced. Indeed, in G1, most models show an anomalous Hadley circulation in which winds aloft, and therefore energy, move towards the summer hemisphere (Figs. 7,8). This is accompanied by anomalous flow towards the winter hemisphere in the lower branch of the Hadley cell, which weakens moisture transport towards the summer hemisphere and moves the summer ITCZ position away from the summer pole. The warming of the winter relative to the summer hemisphere and the ITCZ shift toward the winter hemisphere are correlated between the different models (Fig. 9b,c), and are consistent with the proposed physical mechanism.

Damped seasonal ITCZ migration caused by cooling of the summer hemisphere presents a physical mechanism for the reduction in summer monsoon precipitation in the G1 experiment found by Tilmes et al. (2013), which they had attributed to a weakening of the hydrological cycle. It also provides an explanation for the narrowing of the annual mean ITCZ in the IPSL-CM5A-LR and MPI-ESM-LR models that could not be accounted for by the annual mean dynamics. If this effect were to occur in the real world, it would likely mean a reduction in precipitation in areas that depend on the seasonal extremes of the ITCZ position for their rainfall, in both hemispheres. This is one more reason to be cautious about implementation of solar geoengineering. Future studies should look for this effect in model simulations that include actual aerosol injections, rather than reducing the solar constant, in order to learn more about this potential risk.

3 Conclusions

Hadley circulation changes are the most significant mechanism driving the $P-E$ changes in climate model simulations of uniform solar dimming. While thermodynamic scaling captures the general spatial structure of $P-E$ changes under global warming, it does not explain the large-scale rainfall changes in idealized simulations of solar geoengineering. The roles of thermodynamic scaling and relative humidity changes may be important on studies of smaller scale responses to geoengineering, such as over rainforests or at high latitudes where the CO_2 physiological response and residual temperature anomalies are more important, respectively.

The models can be divided into three groups characterized by different precipitation responses to geoengineering: either a southward shift, northward shift, or narrowing of the ITCZ. Our results support that changes in tropical dynamics, namely shifts of the Hadley circulation, are largely responsible for these alterations to the $P-E$ distribution. In a previous study, convection scheme parameters were determinative of the tropical precipitation response to extratropical forcings (Kang et al., 2009). The partitioning of cross-equatorial fluxes between atmospheric and oceanic components is also important for the resulting ITCZ shift, so differences in the oceanic component of the models could emerge as significant (Kang et al., 2008).

We also present evidence that land-sea contrasts in evaporation rates, resulting in land-sea contrasts in relative humidity anomalies, contribute to small changes in $P-E$ with solar dimming. We propose that these relative humidity changes are related to the effect of CO_2 on the stomatal conductance in plants.

This study demonstrates that tropical precipitation is sensitive to solar perturbations and would be altered by an implementation of solar geoengineering. The basis of this alteration is primarily dynamical. Based on our inter-model comparison, there is substantial uncertainty regarding the nature of the tropical precipitation response, in terms of the direction and strength of the ITCZ shift, as well as its variation on seasonal time scales. We present evidence that residual warming of one hemisphere relative to the other under geoengineering draws annual mean tropical rainfall into that hemisphere. On seasonal timescales, preferential cooling of the summer hemisphere results in a damping of the seasonal migration of the ITCZ, which explains the apparent narrowing of the tropical peak in annual mean precipitation and helps account for the reduction in summer monsoon precipitation found by Tilmes et al. (2013). Our results reinforce the finding that uniform solar dimming cannot restore preindustrial conditions in terms of $P-E$ patterns, a fundamental aspect of climate. An investigation of the ability of spatially targeted solar geoengineering to offset these $P-E$ changes would be a valuable future direction.

Author contributions. T. Storelvmo designed research and J.E. Smyth performed the analysis. J.E. Smyth and T. Storelvmo interpreted results, and J.E. Smyth wrote the manuscript with input from the coauthors. R.D. Russotto contributed Figures 9 and 10 and wrote several paragraphs discussing them.

Acknowledgements. Two anonymous reviewers provided comments which helped to improve the manuscript. We thank the climate modeling groups for participating in the Geoengineering Model Intercomparison Project and for making their data available. In particular we thank Dr.

Ben Kravitz and the scientists managing the Earth System Grid Federation for facilitating data access. T. Storelvmo was supported by NSF under grant 1352417. J.E. Smyth was supported by the Karen Von Damm '77 Undergraduate Research Fellowship from the Yale University Department of Geology & Geophysics. R.D. Russotto was supported in part by the U.S. Department of Defense (DoD) through the National Defense Science and Engineering Graduate Fellowship (NDSEG) Program.

References

Allen, M. R. and Ingram, W. J.: Constraints on future changes in climate and the hydrologic cycle, Nature, 419, 224–232, 2002.

Arora, V. K., Scinocca, J. F., Boer, G. J., Christian, J. R., Denman, K. L., Flato, G. M., Kharin, V. V., Lee, W. G., and Merryfield, W. J.: Carbon emission limits required to satisfy future representative concentration pathways of greenhouse gases, Geophysical Research Letters, 38, L05805, doi:10.1029/2010GL046270, 2011.

Bala, G., Duffy, P., and Taylor, K.: Impact of geoengineering schemes on the global hydrological cycle, PNAS, 105, 7664–7669, 2008.

Bentsen, M., Bethke, I., Debernard, J. B., Iversen, T., Kirkevåg, A., Seland, Ø., Drange, H., Roelandt, C., Seierstad, I. A., Hoose, C., and Kristjánsson, J. E.: The Norwegian Earth System Model, NorESM1-M – Part 1: Description and basic evaluation of the physical climate, Geoscientific Model Development, 6, 687–720, doi:10.5194/gmd-6-687-2013, 2013.

Broccoli, A. J., Dahl, K. A., and Stouffer, R. J.: Response of the ITCZ to Northern Hemisphere cooling, Geophysical Research Letters, 33, doi:10.1029/2005GL024546, http://dx.doi.org/10.1029/2005GL024546, l01702, 2006.

Byrne, M. P. and O'Gorman, P. A.: The Response of Precipitation Minus Evapotranspiration to Climate Warming: Why the "Wet-Get-Wetter, Dry-Get-Drier" Scaling Does Not Hold over Land, Journal of Climate, 28, 8078–8092, doi:10.1175/JCLI-D-15-0369.1, 2015.

Cao, L., Bala, G., Caldeira, K., Nemani, R., and Ban-Weiss, G.: Importance of carbon dioxide physiological forcing to future climate change, Proceedings of the National Academy of Sciences, 107, 9513–9518, doi:10.1073/pnas.0913000107, 2010.

Collins, W. J., Bellouin, N., Doutriaux-Boucher, M., Gedney, N., Halloran, P., Hinton, T., Hughes, J., Jones, C. D., Joshi, M., Liddicoat, S., Martin, G., O'Connor, F., Rae, J., Senior, C., Sitch, S., Totterdell, I., Wiltshire, A., and Woodward, S.: Development and evaluation of an Earth-System model – HadGEM2, Geoscientific Model Development, 4, 1051–1075, doi:10.5194/gmd-4-1051-2011, 2011.

Crutzen, P. J.: Albedo Enhancement by Stratospheric Sulfur Injections: A Contribution to Resolve a Policy Dilemma?, Climatic Change, 77, 211–220, doi:10.1007/s10584-006-9101-y, http://dx.doi.org/10.1007/s10584-006-9101-y, 2006.

Dufresne, J.-L., Foujols, M.-A., Denvil, S., Caubel, A., Marti, O., Aumont, O., Balkanski, Y., Bekki, S., Bellenger, H., Benshila, R., Bony, S., Bopp, L., Braconnot, P., Brockmann, P., Cadule, P., Cheruy, F., Codron, F., Cozic, A., Cugnet, D., de Noblet, N., Duvel, J.-P., Ethé, C., Fairhead, L., Fichefet, T., Flavoni, S., Friedlingstein, P., Grandpeix, J.-Y., Guez, L., Guilyardi, E., Hauglustaine, D., Hourdin, F., Idelkadi, A., Ghattas, J., Joussaume, S., Kageyama, M., Krinner, G., Labetoulle, S., Lahellec, A., Lefebvre, M.-P., Lefevre, F., Levy, C., Li, Z. X., Lloyd, J., Lott, F., Madec, G., Mancip, M., Marchand, M., Masson, S., Meurdesoif, Y., Mignot, J., Musat, I., Parouty, S., Polcher, J., Rio, C., Schulz, M., Swingedouw, D., Szopa, S., Talandier, C., Terray, P., Viovy, N., and Vuichard, N.: Climate change projections using the IPSL-CM5 Earth System Model: from CMIP3 to CMIP5, Climate Dynamics, 40, 2123–2165, doi:10.1007/s00382-012-1636-1, 2013.

Frierson, D. and Hwang, Y.-T.: Extratropical Influence on ITCZ Shifts in Slab Ocean Simulations of Global Warming, Journal of Climate, 25, 720–733, doi:10.1175/JCLI-D-11-00116.1, 2012.

Fyfe, J., Cole, J., Arora, V., and Scinocca, J.: Biogeochemical carbon coupling influences global precipitation in geoengineering experiments, Geophys. Res. Letters, 40, 651–655, 2013.

Gent, P. R., Danabasoglu, G., Donner, L. J., Holland, M. M., Hunke, E. C., Jayne, S. R., Lawrence, D. M., Neale, R. B., Rasch, P. J., Vertenstein, M., Worley, P. H., Yang, Z.-L., and Zhang, M.: The Community Climate System Model Version 4, Journal of Climate, 24, 4973–4991, doi:10.1175/2011JCLI4083.1, 2011.

Giorgetta, M. A., Jungclaus, J., Reick, C. H., Legutke, S., Bader, J., Böttinger, M., Brovkin, V., Crueger, T., Esch, M., Fieg, K., Glushak, K., Gayler, V., Haak, H., Hollweg, H.-D., Ilyina, T., Kinne, S., Kornblueh, L., Matei, D., Mauritsen, T., Mikolajewicz, U., Mueller, W., Notz, D., Pithan, F., Raddatz, T., Rast, S., Redler, R., Roeckner, E., Schmidt, H., Schnur, R., Segschneider, J., Six, K. D., Stockhause, M.,

Timmreck, C., Wegner, J., Widmann, H., Wieners, K.-H., Claussen, M., Marotzke, J., and Stevens, B.: Climate and carbon cycle changes from 1850 to 2100 in MPI-ESM simulations for the Coupled Model Intercomparison Project phase 5, Journal of Advances in Modeling Earth Systems, 5, 572–597, doi:10.1002/jame.20038, 2013.

Gordon, C., Cooper, C., Senior, C. A., Banks, H., Gregory, J. M., Johns, T. C., Mitchell, J. F. B., and Wood, R. A.: The simulation of SST, sea ice extents and ocean heat transports in a version of the Hadley Centre coupled model without flux adjustments, Climate Dynamics, 16, 147–168, doi:10.1007/s003820050010, http://dx.doi.org/10.1007/s003820050010, 2000.

Haywood, J., Jones, A., Bellouin, N., and Stephenson, D.: Asymmetric forcing from stratospheric aerosols impacts Sahelian rainfall, Nature Climate Change, 1857, 1–6, 2013.

Haywood, J. M., Jones, A., Dunstone, N., Milton, S., Vellinga, M., Bodas-Salcedo, A., Hawcroft, M., Kravitz, B., Cole, J., Watanabe, S., and Stephens, G.: The impact of equilibrating hemispheric albedos on tropical performance in the HadGEM2-ES coupled climate model, Geophysical Research Letters, 43, 395–403, doi:10.1002/2015GL066903, http://dx.doi.org/10.1002/2015GL066903, 2015GL066903, 2016.

Hazeleger, W., Wang, X., Severijns, C., Ştefănescu, S., Bintanja, R., Sterl, A., Wyser, K., Semmler, T., Yang, S., van den Hurk, B., van Noije, T., van der Linden, E., and van der Wiel, K.: EC-Earth V2.2: description and validation of a new seamless earth system prediction model, Climate Dynamics, 39, 2611–2629, doi:10.1007/s00382-011-1228-5, 2012.

Held, I.: The Partitioning of the Poleward Energy Transport between the Tropical Ocean and Atmosphere, Journal of the Atmospheric Sciences, 58, 943–948, 2001.

Held, I. and Soden, B.: Robust responses of the hydrological cycle to global warming, Journal of Climate, 19, 5686–5699, 2006.

Hill, S., Ming, Y., and Held, I.: Mechanisms of Forced Tropical Meridional Energy Flux Change, Journal of Climate, 28, 1725–1742, 2015.

Hurrell, J. W., Holland, M. M., Gent, P. R., Ghan, S., Kay, J. E., Kushner, P. J., Lamarque, J.-F., Large, W. G., Lawrence, D., Lindsay, K., Lipscomb, W. H., Long, M. C., Mahowald, N., Marsh, D. R., Neale, R. B., Rasch, P., Vavrus, S., Vertenstein, M., Bader, D., Collins, W. D., Hack, J. J., Kiehl, J., and Marshall, S.: The Community Earth System Model: A Framework for Collaborative Research, Bulletin of the American Meteorological Society, 94, 1339–1360, doi:10.1175/BAMS-D-12-00121.1, 2013.

Hwang, Y.-T., Frierson, D. M. W., and Kang, S. M.: Anthropogenic sulfate aerosol and the southward shift of tropical precipitation in the late 20th century, Geophysical Research Letters, 40, 2845–2850, doi:10.1002/grl.50502, 2013.

IPCC: Climate Change 2014: Impacts, Adaptation, and Vulnerability. Part A: Global and Sectoral Aspects, p. 1132, Cambridge University Press, Cambridge, United Kingdom and New York, NY, USA, 2014.

Ji, D., Wang, L., Feng, J., Wu, Q., Cheng, H., Zhang, Q., Yang, J., Dong, W., Dai, Y., Gong, D., Zhang, R.-H., Wang, X., Liu, J., Moore, J. C., Chen, D., and Zhou, M.: Description and basic evaluation of Beijing Normal University Earth System Model (BNU-ESM) version 1, Geoscientific Model Development, 7, 2039–2064, doi:10.5194/gmd-7-2039-2014, http://www.geosci-model-dev.net/7/2039/2014/, 2014.

Kang, S., Held, I., Friersona, D., and Zhao, M.: The Response of the ITCZ to Extratropical Thermal Forcing: Idealized Slab-Ocean Experiments with a GCM, Journal of Climate, 21, 3521–3532, 2008.

Kang, S., Frierson, D., and Held, I.: The Tropical Response to Extratropical Thermal Forcing in an Idealized GCM: The Importance of Radiative Feedbacks and Convective Parameterization, Journal of the Atmospheric Sciences, 66, 2812–2827, 2009.

Kravitz, B., Robock, A., Boucher, O., Schmidt, H., and Taylor, K.: Specifications for GeoMIP experiments G1 through G4, Available online at http://climate.envsci.rutgers.edu/GeoMIP/docs/specificationsG1G4.pdf [accessed April 2016], 2010.

Kravitz, B., Caldeira, K., Boucher, O., Robock, A., Rasch, P. J., Alterskjær, K., Karam, D. B., Cole, J. N. S., Curry, C. L., Haywood, J. M., Irvine, P. J., Ji, D., Jones, A., Kristjánsson, J. E., Lunt, D. J., Moore, J. C., Niemeier, U., Schmidt, H., Schulz, M., Singh, B., Tilmes, S.,

Watanabe, S., Yang, S., and Yoon, J.-H.: Climate model response from the Geoengineering Model Intercomparison Project (GeoMIP), JGR: Atmospheres, 118, 8320–8332, 2013a.

Kravitz, B., Rasch, P. J., Forster, P. M., Andrews, T., Cole, J. N. S., Irvine, P. J., Ji, D., Kristjánsson, J. E., Moore, J. C., Muri, H., Niemeier, U., Robock, A., Singh, B., Tilmes, S., Watanabe, S., and Yoon, J.-H.: An energetic perspective on hydrological cycle changes in the Geoengineering Model Inter-Comparison Project, JGR: Atmospheres, 118, 13,087–13,102, 2013c.

NRC: Front Matter. Climate Intervention: Reflecting Sunlight to Cool Earth, Washington, DC: The National Academies Press, doi:10.17226/18988, 2015.

Robock, A., Marquardt, A., Kravitz, B., and Stenchikov, G.: Benefits, risks, and costs of solar geoengineering, Geophysical Research Letters, 36, 2009.

Schmidt, G. A., Kelley, M., Nazarenko, L., Ruedy, R., Russell, G. L., Aleinov, I., Bauer, M., Bauer, S. E., Bhat, M. K., Bleck, R., Canuto, V., Chen, Y.-H., Cheng, Y., Clune, T. L., Del Genio, A., de Fainchtein, R., Faluvegi, G., Hansen, J. E., Healy, R. J., Kiang, N. Y., Koch, D., Lacis, A. A., LeGrande, A. N., Lerner, J., Lo, K. K., Matthews, E. E., Menon, S., Miller, R. L., Oinas, V., Oloso, A. O., Perlwitz, J. P., Puma, M. J., Putman, W. M., Rind, D., Romanou, A., Sato, M., Shindell, D. T., Sun, S., Syed, R. A., Tausnev, N., Tsigaridis, K., Unger, N., Voulgarakis, A., Yao, M.-S., and Zhang, J.: Configuration and assessment of the GISS ModelE2 contributions to the CMIP5 archive, Journal of Advances in Modeling Earth Systems, 6, 141–184, doi:10.1002/2013MS000265, 2014.

Schneider, T., Bischoff, T., and Huag, G.: Migrations and dynamics of the intertropical convergence zone, Nature Review, 513, 45–53, 2014.

Seo, J., Kang, S., and Frierson, D.: Sensitivity of Intertropical Convergence Zone Movement to the Latitudinal Position of Thermal Forcing, Journal of Climate, 27, 3035–3042, 2014.

Shekar and Boos: Improving Energy-Based Estimates of Monsoon Location in the Presence of Proximal Deserts, Journal of Climate, 29, 2016.

Sherwood, S. C., Ingram, W., Tsushima, Y., Satoh, M., Roberts, M., Vidale, P. L., and O'Gorman, P. A.: Relative humidity changes in a warmer climate, Journal of Geophysical Research: Atmospheres, 115, doi:10.1029/2009JD012585, 2010.

Simmons, A. J., Willett, K. M., Jones, P. D., Thorne, P. W., and Dee, D. P.: Low-frequency variations in surface atmospheric humidity, temperature, and precipitation: Inferences from reanalyses and monthly gridded observational data sets, Journal of Geophysical Research: Atmospheres, 115, doi:10.1029/2009JD012442, 2010.

Souch, C. and Grimmond, C.: Applied climatology:heat waves', Progress in Physical Geography, 28, 599–606, 2004.

Tilmes, S., Fasullo, J., Lamarque, J.-F., Marsh, D. R., Mills, M., Alterskjær, K., Muri, H., Kristjánsson, J. E., Boucher, O., Schulz, M., et al.: The hydrological impact of geoengineering in the Geoengineering Model Intercomparison Project (GeoMIP), Journal of Geophysical Research: Atmospheres, 118, 2013.

Toggweiler, J. R. and Lea, D. W.: Temperature differences between the hemispheres and ice age climate variability, Paleoceanography, 25, doi:10.1029/2009PA001758, http://dx.doi.org/10.1029/2009PA001758, pA2212, 2010.

Trenberth, K.: Atmospheric Moisture Recycling: Role of Advection and Local Evaporation, Journal of Climate, 12, 1368–1381, 1999.

Watanabe, S., Hajima, T., Sudo, K., Nagashima, T., Takemura, T., Okajima, H., Nozawa, T., Kawase, H., Abe, M., Yokohata, T., Ise, T., Sato, H., Kato, E., Takata, K., Emori, S., and Kawamiya, M.: MIROC-ESM 2010: model description and basic results of CMIP5-20c3m experiments, Geoscientific Model Development, 4, 845–872, doi:10.5194/gmd-4-845-2011, 2011.

Willett, K., Jones, P., Thorne, P., and Gillett, N.: A comparison of large scale changes in surface humidity over land in observations and CMIP3 general circulation models, Environmental Research Letters, 5, 025 210, 2010.

Yoshimori and Broccoli: Equilibrium Response of an Atmosphere–Mixed Layer Ocean Model to Different Radiative Forcing Agents: Global and Zonal Mean Response, J. Atmos. Sci., 21, 4399–4423, 2008.

FIGURES

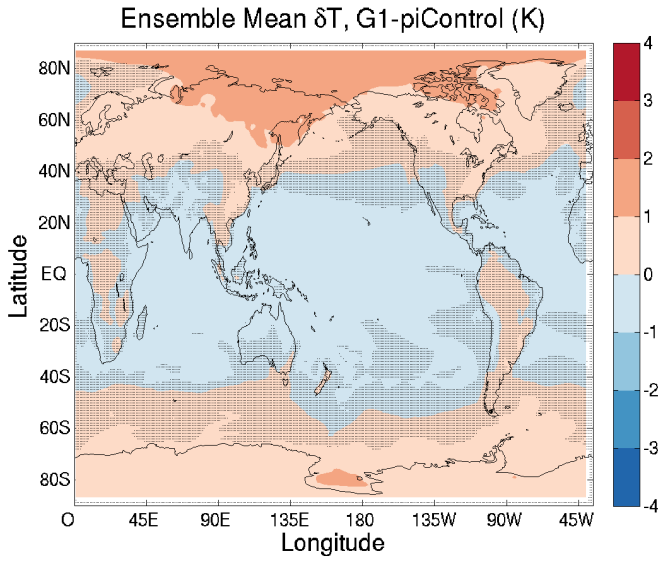

Figure 1. The annual mean distribution of near-surface atmospheric temperature anomalies (K) between G1 (years 11-50) and piControl (all years). Stippling denotes regions where fewer than 66% of the 12 ensemble members agree on the sign of the change. These results appear in Kravitz et al. 2013a.

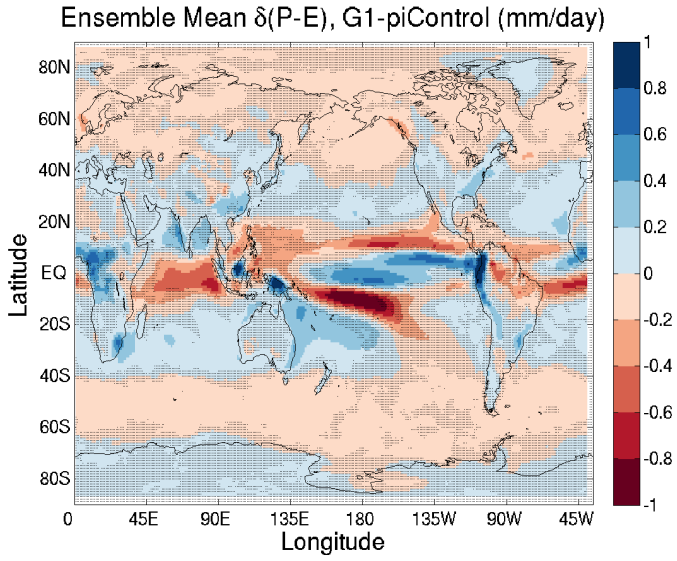

Figure 2. The annual mean distribution of precipitation minus evaporation rate anomalies (mm/year) between G1 (years 11-50) and piControl (all years), averaged among 11 models (EC-Earth excluded due to unphysical result). Stippling indicates where fewer than 64% of models agree on the sign of the change. These results appear in Kravitz et al. 2013a.

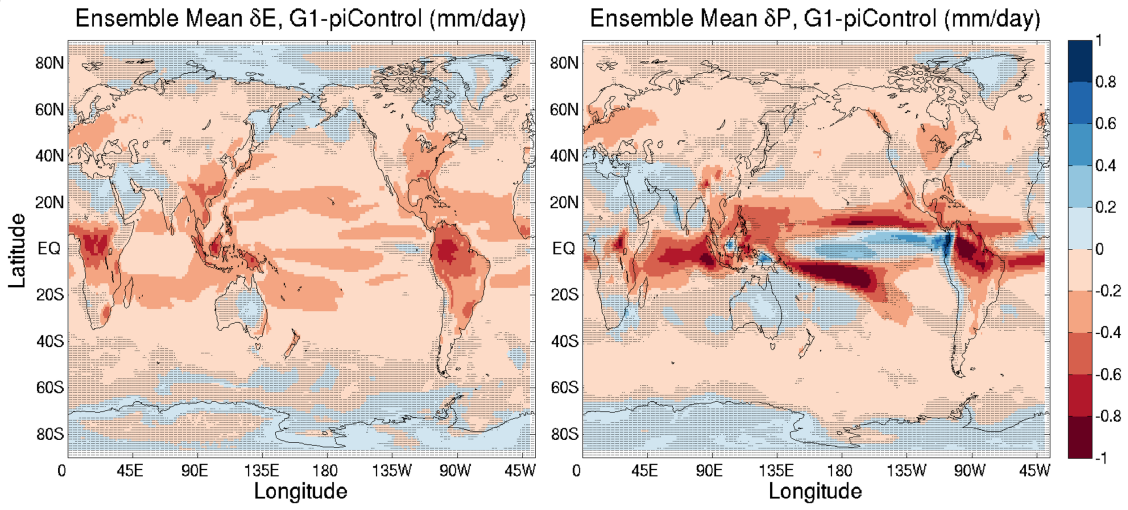

Figure 3. The annual mean distribution of evaporation (left panel) and precipitation (right panel) rate anomalies (mm/year) between G1 (years 11-50) and piControl (all years), averaged among 11 models (EC-Earth excluded due to unphysical result). Stippling indicates where fewer than 64% of models agree on the sign of the change. These results appear in Kravitz et al. 2013a.

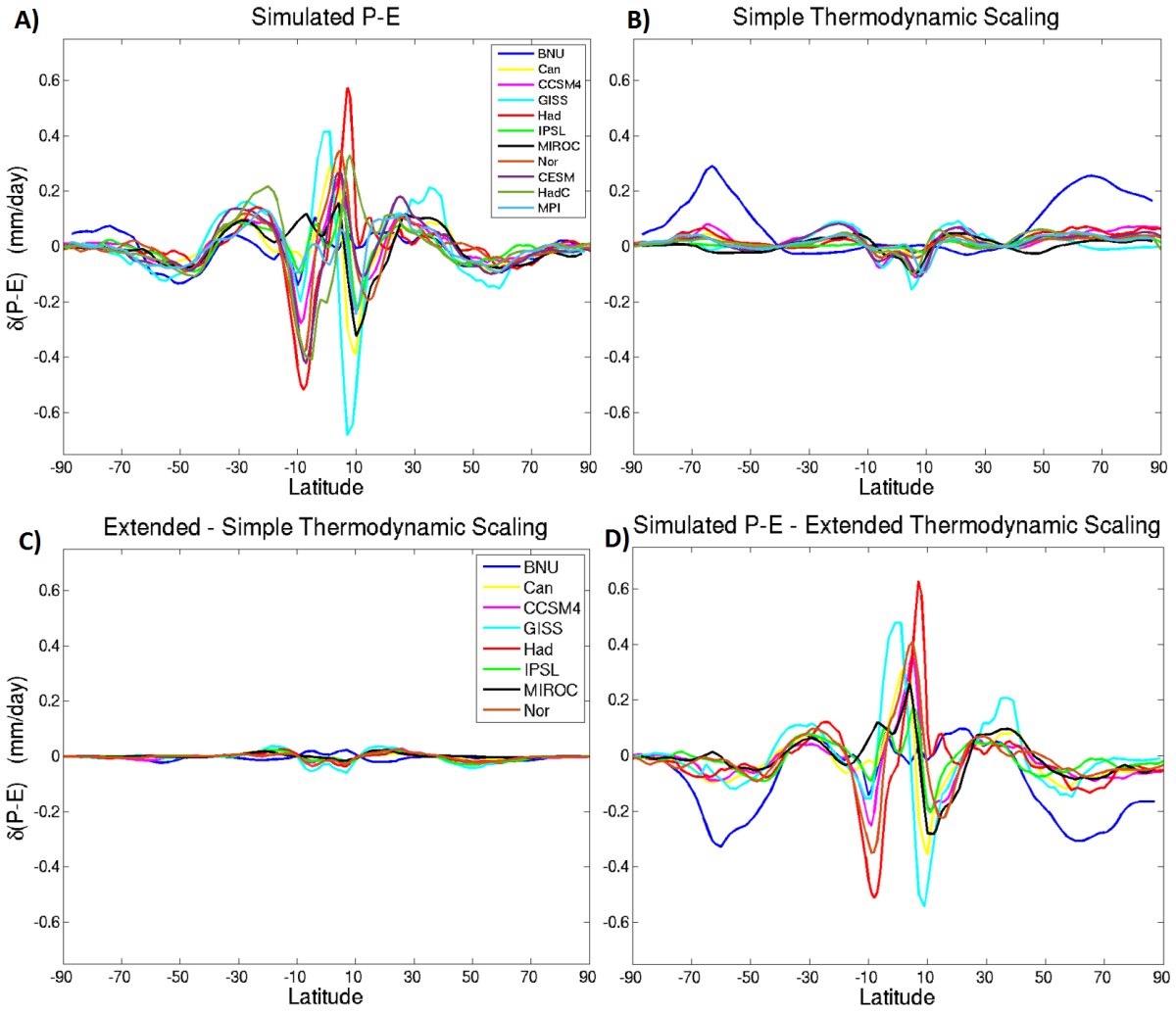

Figure 4. A) shows the zonal mean $P-E$ anomaly G1-piControl simulated in 11 climate models, and B) is the $P-E$ anomaly predicted by the simple thermodynamic scaling in Eq. (2). C) shows the $\delta P-E$ difference between the extended (Eq. (3)) and simple (Eq. (2)) scalings. This isolates the contribution of local relative humidity changes to the $P-E$ anomalies. D) is the difference between the simulated $\delta P-E$ and the extended scaling, and represents the changes in dynamically driven rainfall. (EC-Earth excluded due to unphysical result).

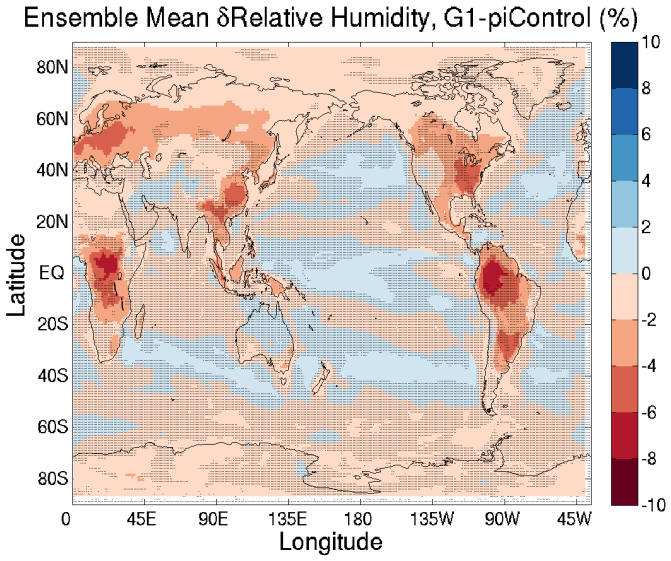

Figure 5. The annual mean near-surface relative humidity anomaly between G1 (years 11-50) and piControl (all years) in eight GCMs. Stippling indicates that fewer than 62.5% of the models agree on the sign of the change. (Data unavailable for HadC, CESM, and MPI models; EC-Earth excluded).

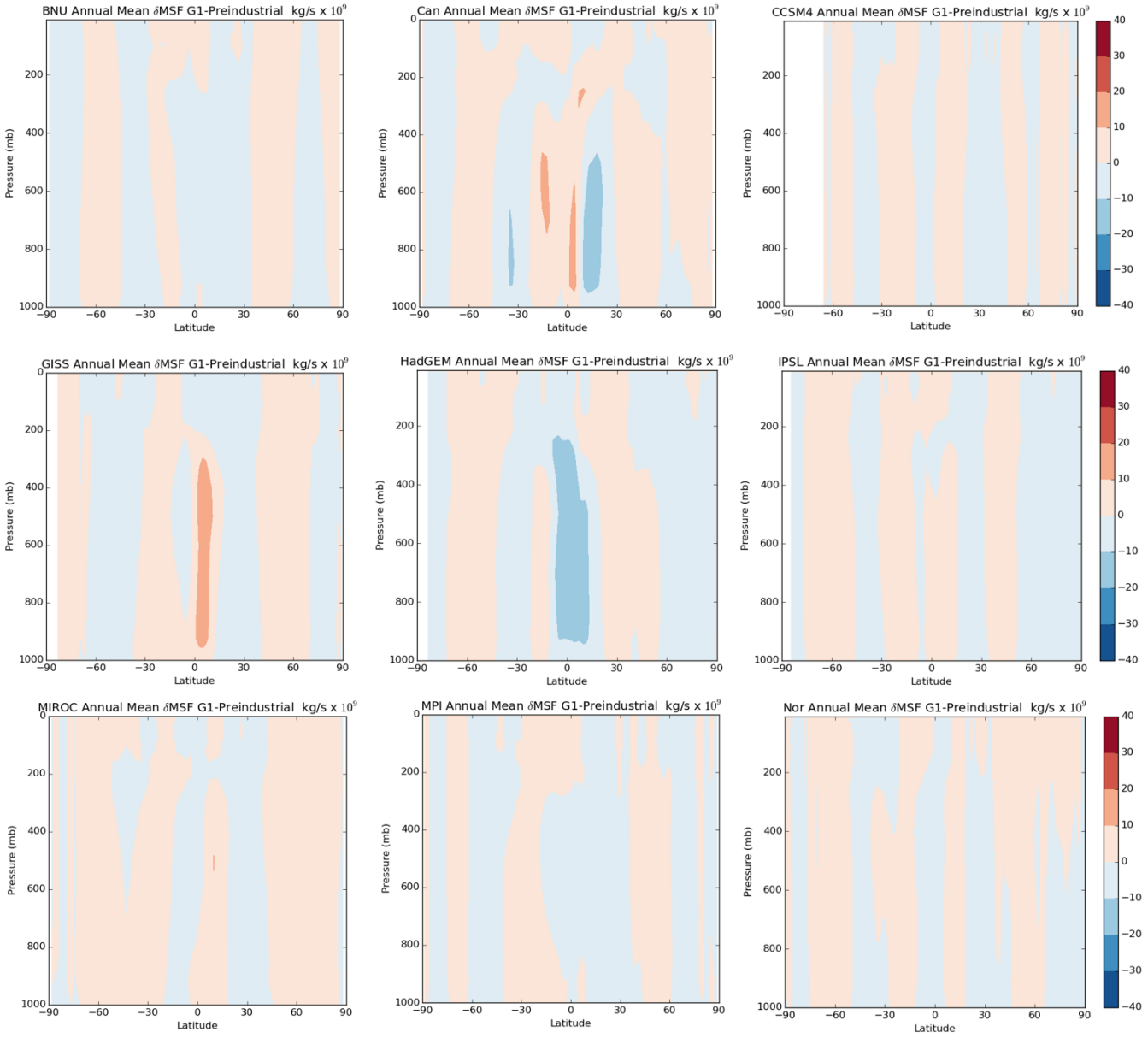

Figure 6. The annual mean meridional streamfunction anomaly between G1 (years 11-50) and piControl (last 40 years) in each model, as calculated in Eq. (4). Blue colors indicate counterclockwise motion. (Data unavailable for HadC and CESM models).

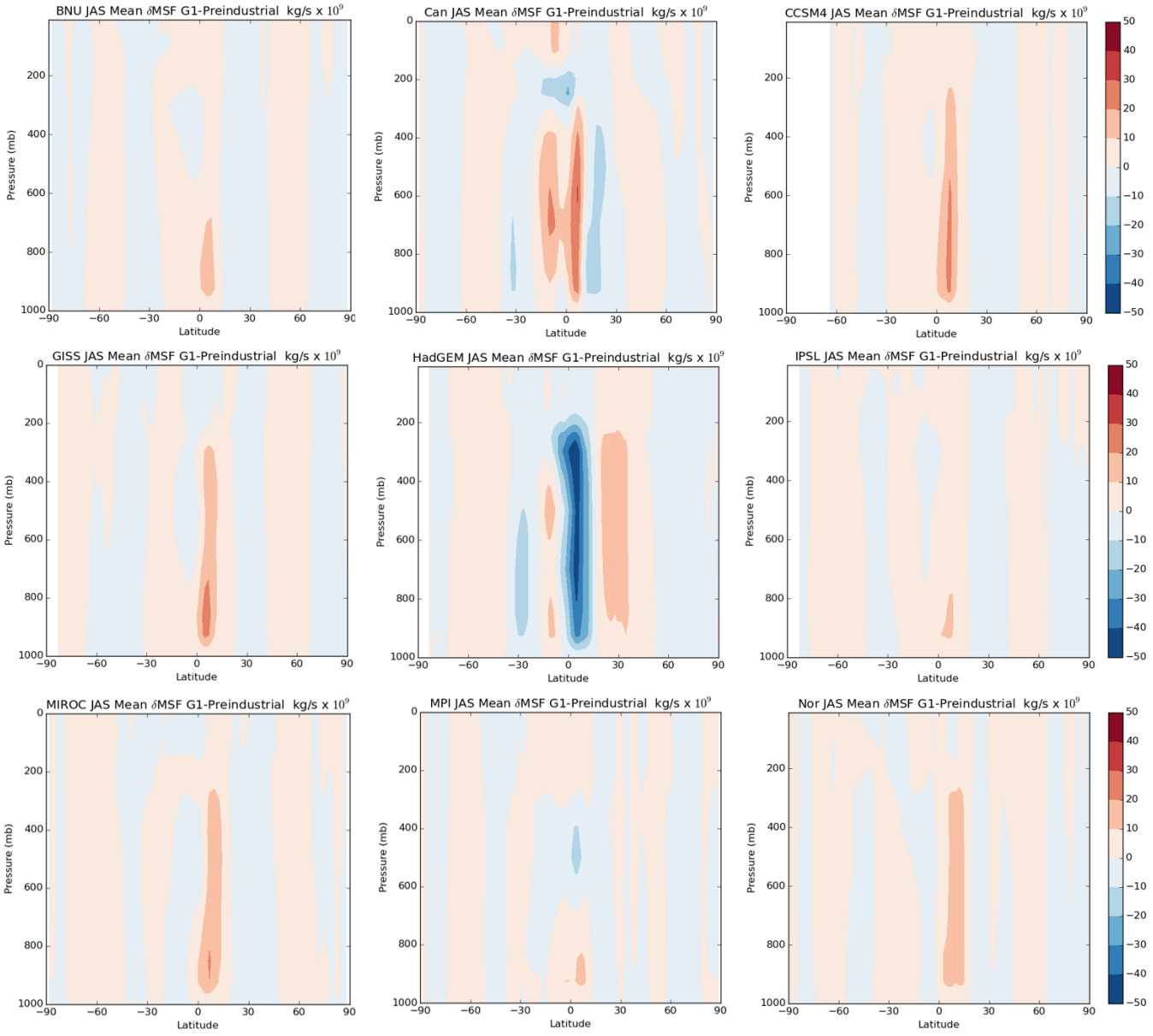

Figure 7. The JAS mean meridional streamfunction anomaly between G1 (years 11-50) and piControl (last 40 years) in each model, as calculated in Eq. (4). Blue colors indicate counterclockwise motion. (Data unavailable for HadC and CESM models).

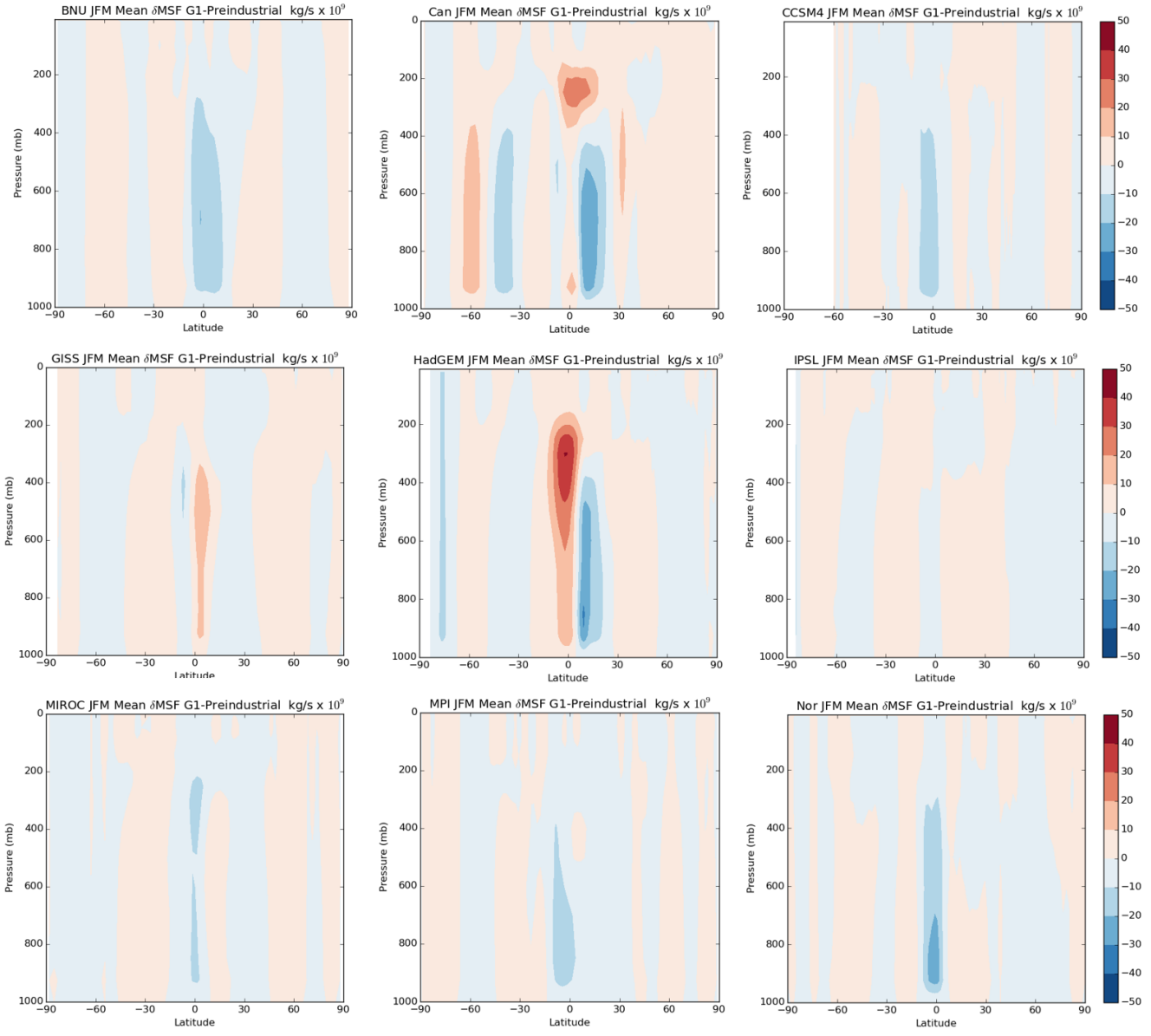

Figure 8. The JFM mean meridional streamfunction anomaly between G1 (years 11-50) and piControl (last 40 years) in each model, as calculated in Eq. (4). Blue colors indicate counterclockwise motion. (Data unavailable for HadC and CESM models).

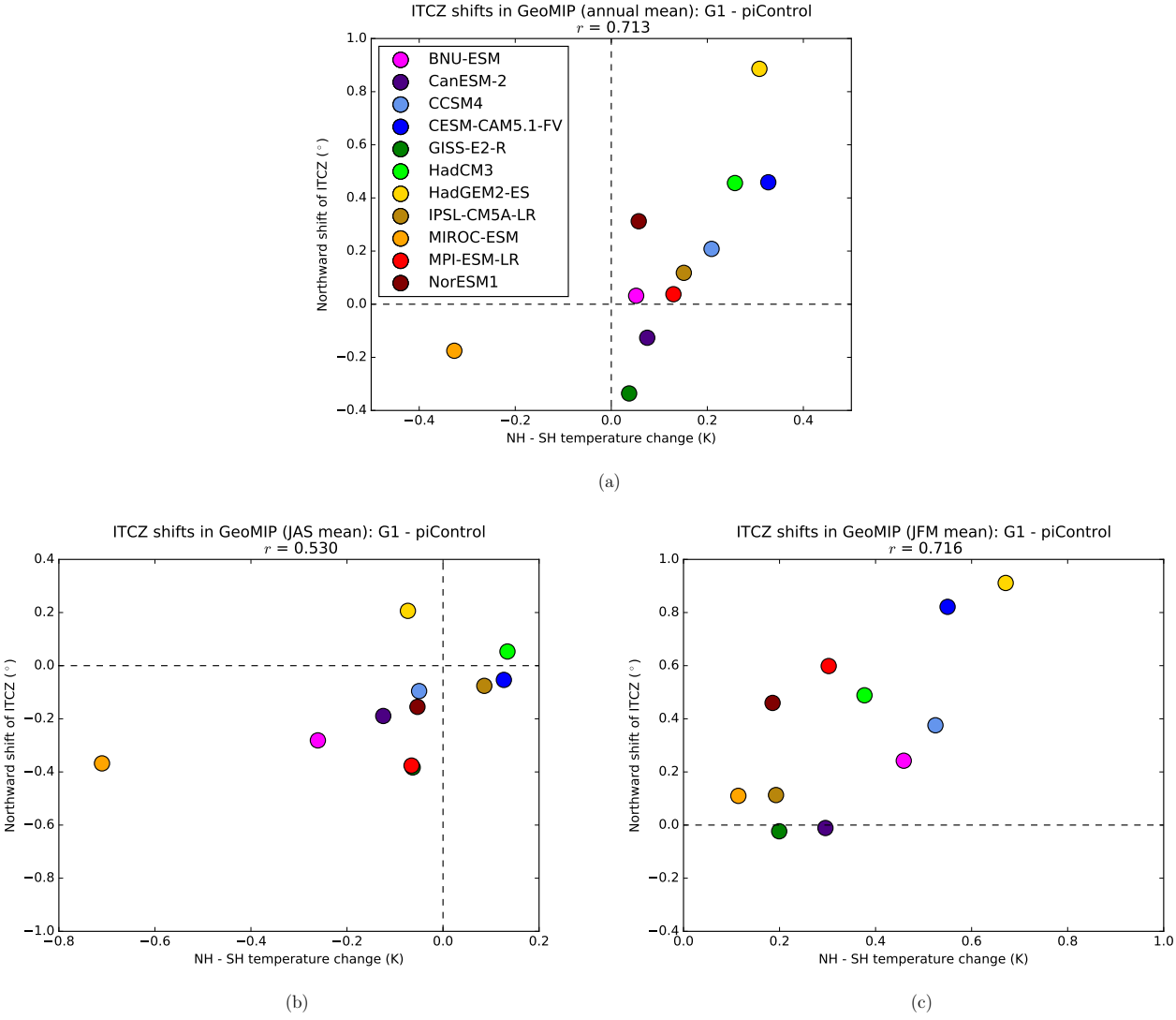

Figure 9. The ITCZ shift vs. the anomaly of the interhemispheric temperature contrast between G1 (years 11-50) and piControl (years 1-40), where r is the correlation coefficient. Panel a) shows the annual mean, b) is the JAS mean, and c) is the JFM mean.

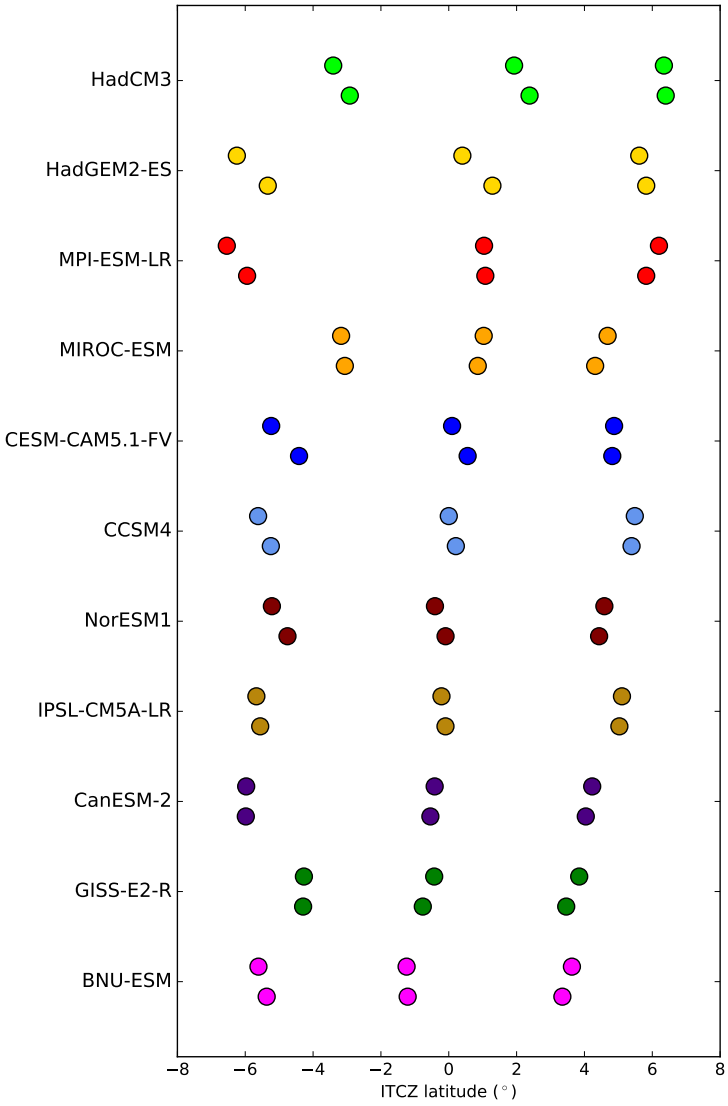

Figure 10. Annual and seasonal mean positions of the ITCZ in piControl (years 1-40) and G1 (years 11-50). For each model, the top row of dots shows piControl positions, and the bottom row of dots shows G1 positions. In each row of dots, the left dot shows the JFM mean position, the middle dot shows the annual mean position, and the right dot shows the JAS mean position. Models are ordered by the annual mean ITCZ position in piControl.

Table 1. GeoMIP Model Specifications. In certain figures models are labeled with the shortened name in parenthesis. Column 3 refers to the CO_2 physiological effect in plants. The solar constant (S_0) reduction is a percentage. Information courtesy of Kravitz et al. (2013a)

Model[1]	Dynamic Vegetation	Phys. Effect	S_0 Reduction	References
BNU-ESM (BNU)	no	yes	3.8	Ji et al. (2014)
Can-ESM2 (Can)	yes	yes	4.0	Arora et al. (2011)
CCSM4 (CCSM4)	no	yes	4.1	Gent et al. (2011)
CESM-CAM5.1-FV (CESM)	no	yes	4.7	Hurrell et al. (2013)
EC-Earth	no	no	4.3	Hazeleger et al. (2012)
GISS-E2-R (GISS)	no	yes	4.5	Schmidt et al. (2014)
HadCM3 (HadC)	no	yes	4.1	Gordon et al. (2000)
HadGEM2-ES (Had)	yes	yes	3.9	Collins et al. (2011)
IPSL-CM5A-LR (IPSL)	yes	yes	3.5	Dufresne et al. (2013)
MIROC-ESM (MIROC)	yes	yes	5.0	Watanabe et al. (2011)
MPI-ESM-LR (MPI)	no	yes	4.7	Giorgetta et al. (2013)
NorESM1-M (Nor)	no	yes	4.0	Bentsen et al. (2013)

1. Full Names: BNU-ESM, Beijing Normal University-Earth System Model; CanESM2, The Second Generation Canadian Earth System Model; CESM-CAM5.1, The Community Climate System Model Version 5.1; CCSM4, The Community Climate System Model Version 4; EC-EARTH DMI, European Earth System Model based on ECMWF Models (Seasonal Forecast System), Danish Meteorological Institute; GISS-E2-R, Goddard Institute for Space Studies ModelE version 2; HadCM3, Hadley Centre coupled model 3; IPSL-CM5A-LR, Institut Pierre Simon Laplace ESM; MIROC-ESM, Model for Interdisciplinary Research on Climate-Earth System Model; MPI-ESM-LR, Max Planck Institute ESM; NorESM1-M, Norwegian ESM.